Journal of Medicinal Chemistry

Article

pubs.acs.org/jmc

Discovery and Optimization of a Porcupine Inhibitor

Athisayamani Jeyaraj Duraiswamy,[†,§] May Ann Lee,[†] Babita Madan,[‡] Shi Hua Ang,[†] Eldwin Sum Wai Tan,[†] Wei Wen Vivien Cheong,[†] Zhiyuan Ke,[†] Vishal Pendharkar,[†] Li Jun Ding,[†] Yun Shan Chew,[†] Vithya Manoharan,[†] Kanda Sangthongpitag,[†] Jenefer Alam,[†] Anders Poulsen,[†] Soo Yei Ho,*[,†] David M. Virshup,[‡] and Thomas H. Keller[†]

[†]Experimental Therapeutics Centre, 31 Biopolis Way, No. 03-01 Nanos, 138669, Singapore

[‡]Duke-NUS Graduate Medical School Singapore, 8 College Road, 169857, Singapore

Supporting Information

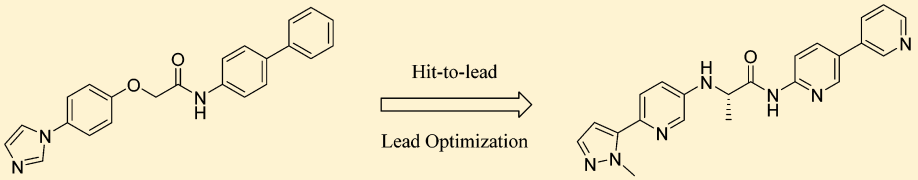

Hit with poor physicochemical properties

Novel chemotype with oral bioavailability

ABSTRACT: Wnt proteins regulate various cellular functions and serve distinct roles in normal development throughout life. Wnt signaling is dysregulated in various diseases including cancers. Porcupine (PORCN) is a membrane-bound *O*-acyltransferase that palmitoleates the Wnts and hence is essential for their secretion and function. The inhibition of PORCN could serve as a therapeutic approach for the treatment of a number of Wnt-dependent cancers. Herein, we describe the identification of a Wnt secretion inhibitor from cellular high throughput screening. Classical SAR based cellular optimization provided us with a PORCN inhibitor with nanomolar activity and excellent bioavailability that demonstrated efficacy in a Wnt-driven murine tumor model. Finally, we also discovered that enantiomeric PORCN inhibitors show very different activity in our reporter assay, suggesting that such compounds may be useful for mode of action studies on the PORCN *O*-acyltransferase.

INTRODUCTION

Wnts are secreted glycoproteins that act as growth factors and regulate various cellular functions[1] including proliferation,[2] differentiation,[3] death,[4] migration and polarity,[5] through the activation of multiple intracellular signaling cascades by binding to various receptors including Frizzleds. There are 19 human Wnt proteins and 10 Frizzled (Fzd) receptors, all exhibiting unique expression patterns and serving distinct roles in normal development and throughout life.[6] This complexity has hampered progress toward viable therapeutics, even though aberrant Wnt signaling is associated with a number of diseases. The canonical Wnt-induced activation of the β-catenin-TCF transcriptional complexes holds promise for drug discovery, since dysregulation of this pathway has been implicated in neurological diseases, inflammatory and fibrotic diseases, metabolic diseases, and a variety of cancers.[6]

During biosynthesis, Wnt ligands undergo palmitoleation by Porcupine (PORCN), a membrane-bound *O*-acyltransferase enzyme that is specifically required for the acylation of newly synthesized Wnt ligands in the endoplasmic reticulum (ER).[7] Palmitoleated Wnt ligands then undergo glycosylation in the ER-Golgi system before secretion.[8] Once outside the cell, Wnt glycoproteins bind to receptors formed by Frizzleds and LRP5/6 co-receptors,[9] resulting in phosphorylation of the Dishevelled protein. In the canonical Wnt pathway this eventually leads to the disruption of the β-catenin degradation complex consisting of AXIN, GSK3, APC, and CK1α and translocation of β-catenin into the nucleus where it forms a complex with LEF/TCF to drive downstream gene expression.[9,10]

The development of small molecules targeting Wnt-secretion or Wnt-signaling may be beneficial for the treatment of cancer[11] or fibrotic diseases.[6] While a number of tool compounds are available, clinical candidates have only recently emerged but none of them have reached the later stages of clinical development.[6] Our approach to disrupt Wnt signaling was to block the secretion of all Wnt proteins through inhibition of a key biosynthetic enzyme, Porcupine (PORCN). Inhibitors of this enzyme have also been pursued by other research groups, and a few tool compounds that inhibit PORCN activity with nanomolar activity (e.g., **1** (IWP-L6),[12,13] Figure 1) have been reported. Novartis disclosed the PORCN inhibitors **2** (C59)[11] and **3** (LGK974)[14] (Figure 1), the latter having reached the stage of a proof or concept clinical trial (ClinicalTrials.gov NCT01351103).

Herein, we describe the identification of a Wnt secretion inhibitor from cellular high throughput screening. The hit was characterized and optimized to develop a potent PORCN inhibitor with excellent bioavailability and good in vivo efficacy

Received: March 30, 2015

DOI: 10.1021/acs.jmedchem.5b00507
J. Med. Chem. XXXX, XXX, XXX−XXX

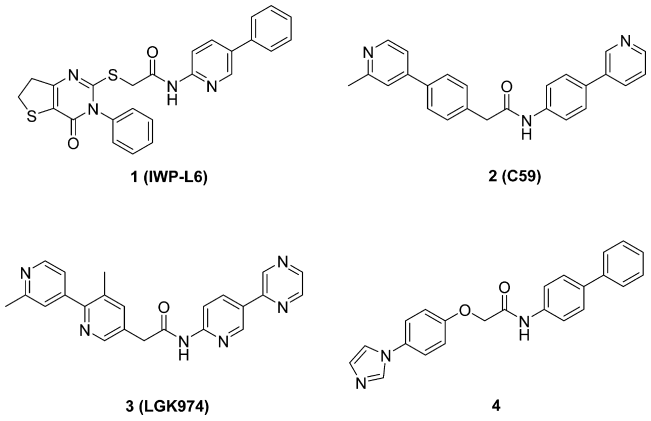

Figure 1. Structures of published PORCN inhibitors and hit **4**.

in a Wnt-dependent murine mammary cancer model, MMTV-Wnt1.

CHEMISTRY

The achiral Wnt pathway modulators were synthesized as shown in Scheme 1. [1,1′-Biphenyl]-4-amine was coupled with chloro- or bromoacetyl chloride in the presence of triethylamine, providing intermediate **5**, which was further reacted with substituted phenols in the presence of K_2CO_3 to give the final compounds **4** and **6**−**10**. Substituted aminoacetamide **11** was synthesized using the same reaction sequence described in Scheme 1.

The two enantiomers of **14** were synthesized starting with ethyl lactate (**12**) (Scheme 2). Mitsunobu reaction with *p*-imidazophenol provided the intermediate **13**, which after hydrolysis of the ethyl ester was coupled with [1,1′-biphenyl]-4-amine. The conformationally restricted proline derivatives were prepared as described in Scheme 3. (*S*)-Proline or (*R*)-proline were N-arylated with dibromobenzene in the presence of CuI to yield intermediates **15**, which were coupled with [1,1′-biphenyl]-4-amine giving the amides **16**. Finally copper-catalyzed reaction of the bromo substituent with imidazole in DMSO provided the chiral proline derivatives (*S*)-**17** and (*R*)-**17**. The chiral integrity of the compounds was maintained during the last step, despite the relatively strong basic conditions (see Experimental Section and Supporting Information Figure S9).

Compound **20** was synthesized in racemic form, and then the enantiomers were separated by chiral HPLC (Scheme 4). The reaction of 4-bromoaniline and ethyl 2-bromopropanoate provided the intermediate **18**, which undergoes copper-catalyzed reaction with imidazole to yield intermediate **19**. Hydrolysis of the ester group followed by amidation yielded the chiral alanine derivatives (*S*)-**20** and (*R*)-**20**.

Compounds **25**−**27** were synthesized in racemic form, and then the enantiomers were separated by chiral HPLC. The synthesis (Scheme 5) of these three compounds started with the Suzuki reaction of 2-bromo-5-nitropyridine with 1-methyl-5-(4,4,5,5-tetramethyl-1,3,2-dioxaborolan-2-yl)-1*H*-pyrazole providing the intermediate **21**. Then the nitro group was reduced and the resulting aniline reacted with ethyl 2-bromopropanoate yielding racemic ester **23**. Hydrolysis of the ester group provided compound **24**. Generally amide couplings between acid **24** and anilines do not proceed well, and it is often advisible to use the corresponding *N*-oxides for this reaction, as demonstrated for the synthesis of **26** and **27** (Scheme 5).

RESULTS AND DISCUSSION

Lead Finding and Hit Evaluation. PORCN is a membrane bound *O*-acyltransferase that so far has not yielded a biochemical assay suitable for high throughput screening, leaving cellular pathway screening as the only alternative. A HEK293-STF cell line[15] that expresses Wnt3A and contains a luciferase reporter for *β*-catenin mediated transcriptional activation was employed for high throughput screening (HTS) of 226 000 compounds. In order to eliminate hits that act downstream of surface receptor activation by Wnt (e.g., tankyrase inhibitors), a second assay was performed. In this case a HEK293-STF cell line without Wnt3A expression was used and screening was done in the presence of Wnt-conditioned medium[16] (HEK293-STF/Wnt) (for a schematic that explains the screening strategy[12] see Supporting Information Figure S1). Hits that were active in the second assay were eliminated from consideration and the remaining compounds examined for general cytotoxicity. Compounds that passed these hurdles and exhibited IC_{50}'s of <100 nM were further evaluated for advancement to the hit-to-lead stage (see Figure S2 for the HTS flowchart). One of the most potent hits **4** displayed an interesting profile with a cellular IC_{50} of 19 nM and a molecular weight of 369 g/mol. Physicochemical parameters were suboptimal (Table 1); however, it was thought that the low solubility and the cytochrome P450 (Cyp) inhibition could be improved during the optimization and the molecular weight suggested that the permeability and bioavailability issues were likely due to the limited solubility of the chemical starting point.

A comparison of the low energy conformations of HTS hit **4** and the known PORCN inhibitors **3** and **1** (Figure 2) suggests that the three inhibitors fit into a common pharmacophore.[17] All three compounds are substituted acetamides, and the

Scheme 1. Synthesis of Compounds 4 and 6−10[a]

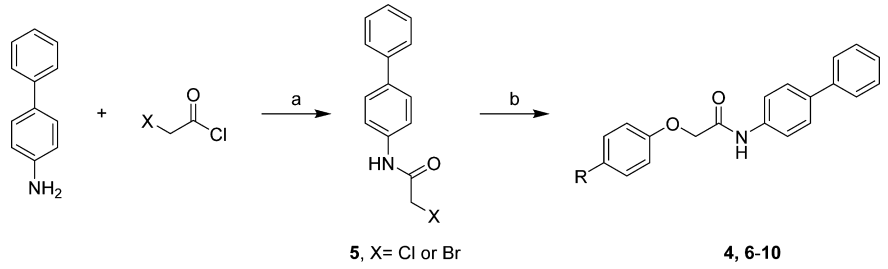

[a]Reagents and conditions: (a) $NaHCO_3$, dioxane, chloro- or bromoacetyl chloride, rt, 16 h; (b) substituted phenol, DMF, K_2CO_3, NaI, rt, 16 h.

DOI: 10.1021/acs.jmedchem.5b00507
J. Med. Chem. XXXX, XXX, XXX−XXX

Scheme 2. Synthesis of the *R*- and *S*-Enantiomers of 14[a]

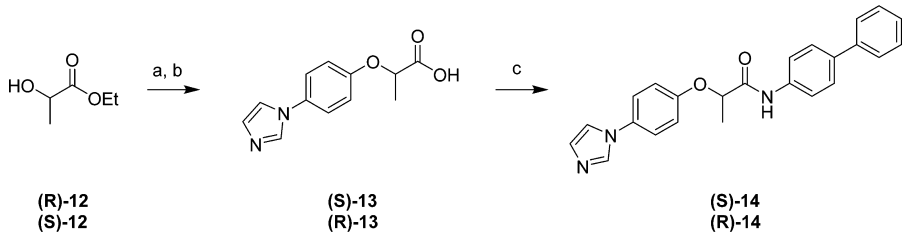

[a]Reagents and conditions: (a) *p*-imidazophenol, diisopropyl azodicarboxylate, Ph_3P, THF, rt, 16 h; (b) LiOH, MeOH, THF, water, rt, 4 h; (c) [1,1′-biphenyl]-4-amine, HATU, $(^iPr)_2NEt$, rt, 16 h.

Scheme 3. Synthesis of the Proline Derivatives (*R*)-17 and (*S*)-17[a]

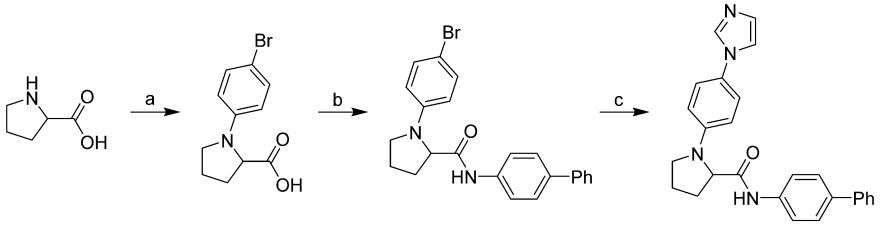

[a]Reagents and conditions: (a) *p*-dibromobenzene, CuI, K_2CO_3, 140 °C, 16 h; (b) [1,1′-biphenyl]-4-amine, HATU, $(^iPr)_2NEt$, rt, 16 h; (c) CuI, imidazole, Cs_2CO_3, DMSO, 90 °C, 16 h.

Scheme 4. Synthesis of the Alanine Derivatives (*R*)-20 and (*S*)-20[a]

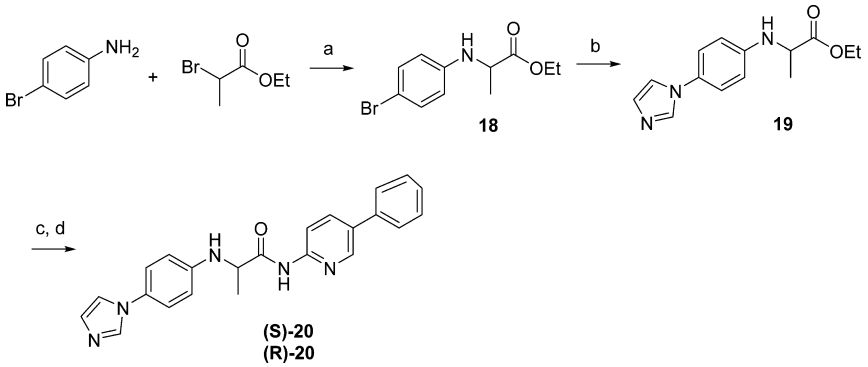

[a]Reagents and conditions: (a) K_2CO_3, 70 °C, 16 h; (b) imidazole, CuI, L-proline, Cs_2CO_3, 90 °C, 16 h; (c) LiOH, 1:1:1 THF−H_2O−MeOH, rt, 2 h; (d) 5-phenylpyridin-2-amine, HATU, *N*-methylmorpholine, DMF, rt, 16 h.

pharmacophore elements of the biaryl and heterobiaryl substituents on the amide overlap very well (see Supporting Information Figure S6). The similarity of the substituents on the -CH_2- group is less obvious, but an analysis of the pharmacophore model[17] in Figure 2 suggests that the terminal pyridine nitrogen of **3** and the imidazole nitrogen of **4** serve as hydrogen bond acceptors in PORCN, while the heterocyclic carbonyl atom of **1** likely uses a water molecule (denoted by the plum pharmacophore element in Figure 2) to make the same interaction with the PORCN protein.

To confirm the hypothesis that **4** is a PORCN inhibitor, a cellular assay was developed to determine whether **4** can inhibit the palmitoleation of Wnt proteins. In this assay exogenous V5-tagged Wnt3a[18] is overexpressed in HeLa cells and cultured in medium containing hexadec-15-ynoic acid (ω-alkynyl palmitate). When the cells are cultured, the PORCN acylates the V5-tagged Wnt3a with ω-alkynyl palmitate, and this modified protein can then be reacted (in the cell lysate) with biotin azide through copper-catalyzed azide−alkyne cycloaddition.[19] The total Wnt3a or palmitoleated Wnt3a can then be detected using an anti-V5 antibody or a streptavidin conjugated dye, respectively. Figure 3 depicts the Western blot demonstrating that **4** blocks the palmitoleation of Wnt3A, consistent with its inhibition of PORCN activity.

Lead Optimization. Having established that **4** is a PORCN inhibitor, the initial stages of the optimization were focused on the imidazole substituent that likely is responsible for the potent Cyp inhibition (Table 2). Nitrogen heterocycles often interact with the heme active site of the Cyp,[20] leading to potent inhibition. The emerging structure−activity relationship (SAR) clearly indicated that the terminal nitrogen is essential for activity in our assay (e.g., **6**). This is also supported by our pharmacophore model[17] (Figure 2). Nevertheless it was possible to remove the undesired activity on the Cyp enzymes by modulating the steric and electronic environment around the terminal nitrogen. Both the oxazole **7** and the *N*-

DOI: 10.1021/acs.jmedchem.5b00507
J. Med. Chem. XXXX, XXX, XXX−XXX

Scheme 5. Synthesis of Compounds 25, 26, and 27[a]

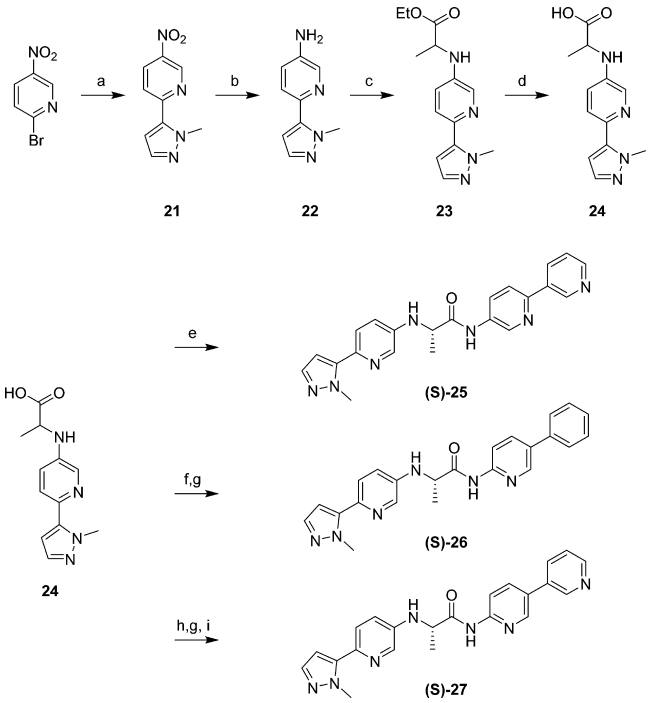

[a]Reagents and conditions: (a) 1-methyl-5-(4,4,5,5-tetramethyl-1,3,2-dioxaborolan-2-yl)-1*H*-pyrazole, $Pd(PPh_3)_4$, K_3PO_4, 100 °C, 16 h; (b) H_2, 10% Pd/C, EtOAc, rt, 12 h; (c) ethyl bromopropionate, NaOAc, ACN, reflux, 48 h; (d) LiOH, 1:1:1 THF−H_2O−MeOH, rt, 2 h; (e) 2,3′-bipyridin-5-amine, HATU, DIPEA, rt, 16 h; (f) 2-amino-5-phenylpyridine 1-oxide, HATU, DIPEA, rt, 16 h; (g) Fe, AcOH, reflux, 2 h; (h) 2-amino-5-bromopyridine 1-oxide, HATU, DIPEA, DMF, rt, 16 h; (i) pyridine-3-boronic acid, $Pd(dppf)Cl_2$.DCM, K_3PO_4, 4:1 dioxane−H_2O, 100 °C, 16 h.

Table 1. Profile of HTS Hit 4

assay/property	value
HEK293-STF[a] (μM)	0.019[b]
HEK293-STF/Wnt[a] (μM)	>30[b]
CC_{50}[a] (μM)	>50[b]
molecular weight (g/mol)	369.4
solubility (μg/mL)	<1
PAMPA, pH 7.4 (10^{-6} cm/s)	<1[c]
CYP[d] 3A4, 2D6 inhibition (μM)	0.02/0.1
mouse oral bioavailability (%)	<1[c]

[a]See Experimental Section. [b]Average of three determinations. [c]May have been impacted by poor solubility. [d]Cytochrome P450 enzyme.

methylpyrazole **10** were devoid of activity on the Cyp enzymes, but the latter was clearly more attractive with single digit nanomolar activity in the Wnt secretion assay. While the discussed modifications (Table 2) improved the side effect profile of the scaffold, solubility was not impacted by these changes (see Supporting Information Table S1).

Two strategies can be considered to improve solubility in drug candidates: (a) reduce the lipophilicity of the compounds; (b) disrupt solid state interactions that are the cause of low intrinsic solubility.[21] During the optimization, we attempted to disrupt crystal packing interactions via the addition of substitutuents around the linker (Table 3).

In the present case, the chiral center had no influence on the solubility at pH 7.4 (see Supporting Information Table S1);

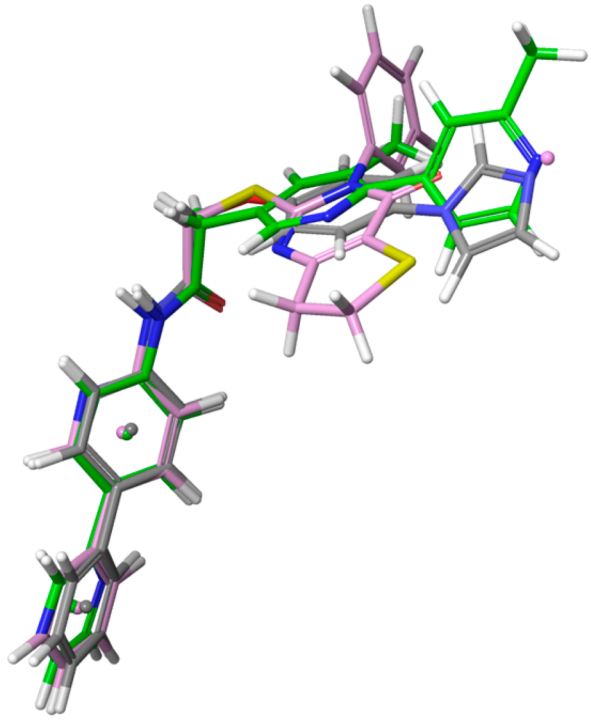

Figure 2. Putative bioactive conformation of **4** (gray carbon), **3** (green carbon), and **1** (plum carbon) superimposed. A site point (plum ball) was constructed 2.8 Å from the oxygen atom (red) in the direction of the carbonyl lone pair on **1**. The site point overlays well with the pyridine acceptor of **3** and imidazole acceptor of **4**.[17]

however we observed a clear effect on the biological activity. With the lactate linker (**14**, Table 3) the *S*-enantiomer is about 20-fold more active than the *R*-enantiomer, an effect that could also be observed in the palmitoleation assay (Figure 3). The chiral discrimination is more pronounced with the more rigid proline derivatives (**17**) leading to a >500-fold difference in biological activity again in favor of the *S*-enantiomer (Table 3). Since the introduction of a chiral center did not have the desired effect, the decision was taken to reduce the clogP, which is 4.5 for (*S*)-**14**. As a first step we synthesized (*S*)-**20** which exhibited a clogP of 3.1. Gratifyingly potency was retained (Table 3) and both microsomal stability and solubility (Supporting Information Table S1) were improved. At this point of the optimization we introduced the *N*-methylpyrazole (see Table 2) into the scaffold and further reduced the clogP with the judicious introduction of further aromatic nitrogens (Table 4). Overall the introduction of the nitrogen atoms led to a sizable reduction in clogP, providing compounds with good solubility and good overall physical properties (Table 4). Compound (*S*)-**27**, with a molecular weight of 400 g/mol, exhibits both good solubility and permeability, suggesting that the low PAMPA value and the limited bioavailability of hit **4** might have been caused by the low solubility. The optimized inhibitor (*S*)-**27** displays good in vivo pharmacokinetics as shown in Table 5 (see also Supporting Information Figure S7).

As discussed previously, the hit evaluation suggested that the chemical starting point **4** is a PORCN inhibitor, and Figure 3 shows that the optimization did not affect the mechanism of the compound. (*S*)-**27** inhibits the palmitoleation of Wnt proteins (Figure 3) with similar potency as the literature compound **2**.[11] Further evidence that (*S*)-**27** is a potent PORCN inhibitor was provided by a cell line overexpressing this Wnt acyltransferase.

DOI: 10.1021/acs.jmedchem.5b00507
J. Med. Chem. XXXX, XXX, XXX−XXX

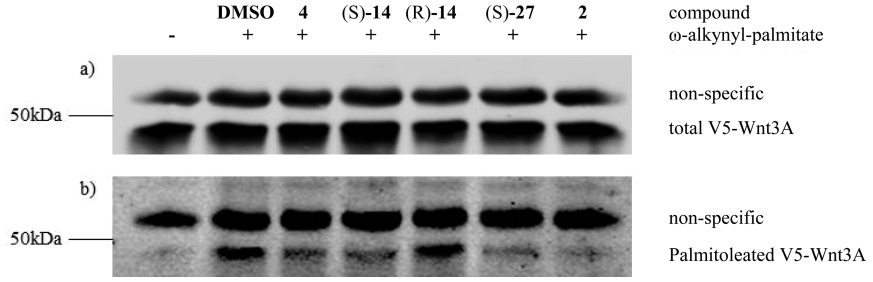

Figure 3. Inhibition of Wnt palmitoleation by Wnt secretion inhibitors in HeLa cells. (a) Total V5-Wnt3A visualized using an anti-V5 antibody followed by anti-mouse Dylight 680. (b) Palmitoleated V5-Wnt3A is reacted in the cell lysate with biotin azide and then detected with streptavidine-Dylight 800.

Table 2. Imidazole SAR

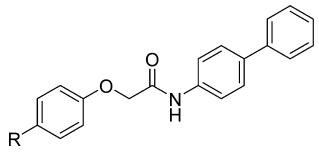

	R	STF3A[a] IC_{50} (μM)	Cyp inhibition 3A4/2D6 IC50 (μM)
4		0.015	0.02/0.1
6		>50	n.d.[b]
7		0.042	>20/>20
8		>50	n.d.[b]
9		0.002	5.2/1.9
10		0.004	>20/>20

[a]Data represent mean value of triplicate experiments. [b]n.d. = not determined.

Table 3. Optimization of the Glycolate Linker

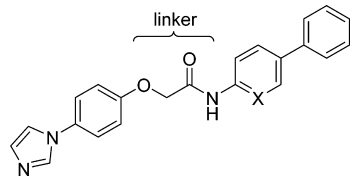

	Linker	X	STF3A IC_{50}[a] (μM)	MLM[b] Cl'int (μl/min/mg)
4	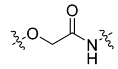	C	0.015	37
11	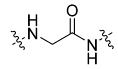	C	0.03	11
(R)-14	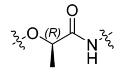	C	0.13	63
(S)-14	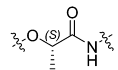	C	0.007	85
(R)-17	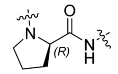	C	33	n.d[c]
(S)-17	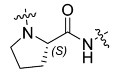	C	0.04	18
(R)-20	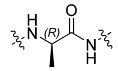	N	0.689	12
(S)-20	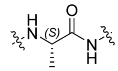	N	0.005	3.5

[a]Data represent mean value of triplicate experiments. [b]Mouse liver microsomes. [c]Not determined.

For this experiment wild type HT1080 cells were treated with either a control plasmid or a murine PORCN expression plasmid in combination with a Wnt/β-catenin reporter plasmid and Wnt3a. Treatment of the wild-type cells with (*S*)-**27** led to a dose dependent inhibition of the luciferase activity, while cells overexpressing PORCN blunted the effect of the inhibitor (Figure 4).

The in vivo efficacy of (*S*)-**27** was tested in a well-established Wnt-driven murine tumor model. For this purpose MMTV-Wnt1 tumor fragments were implanted in the mammary fat pads of Balb/c nude mice. After 14 days, mice bearing established MMTV-Wnt1 tumors were treated with vehicle or three different doses of (*S*)-**27** by oral gavage. For comparison one group of animals received 3 mg/kg of **2**, a compound that previously had been shown to prevent tumor growth in this animal model.[11] Figure 5 shows that (*S*)-**27** inhibited tumor growth in a dose-dependent manner and with similar potency as **2** (for a comparison of the in vitro pharmacokinetic profile of **2** and (*S*)-**27** see Supporting Information Table S3). The percentage of tumor growth inhibition was statistically significant at all three doses and ranged from 50% to 91% (Figure 5).

CONCLUSION

Modulation of aberrant Wnt signaling is becoming a very attractive drug discovery strategy for cancer, vascular disease, and tissue fibrosis. Unfortunately, the progress toward viable therapeutics has been rather slow, mainly because of the complexity of Wnt signaling and the dearth of tool compounds to dissect the pathway.

DOI: 10.1021/acs.jmedchem.5b00507
J. Med. Chem. XXXX, XXX, XXX−XXX

Table 4. Optimization of Physical Properties

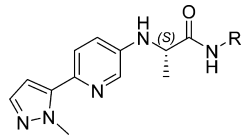

	R	cLogP[a]	STF3A[b] IC_{50} (μM)	Cyp 3A4/2D6 inhibition IC_{50} (μM)	Solubility[c] (μg/ml)	PAMPA[d] (10^{-6} cm/sec)	MLM[e] Cl'int (μl/min/mg)
(S)-**26**		2.6	0.001	>20/>20	4	112.9	8
(S)-**25**		1.8	0.010	>20/3.3	102	26.8	8
(S)-**27**		1.8	0.001	>20/8	72.5	50.6	8

[a]Determined using Stardrop. [b]Data represent mean value of triplicate experiments. [c]Thermodynamic solubility at pH 7.4. [d]Determined at pH 7.4. [e]Mouse liver microsomes.

Table 5. In Vivo Pharmacokinetics[a] for (*S*)-27

	F (%)	C_{max} (ng/mL)	$T_{1/2}$ (h)	$AUC_{0-t(last)}$ (ng·h/mL)
(*S*)-**27**	106	4268	1.9	12266

[a]Mouse. Dose of 1 mg/kg for iv studies and 5 mg/kg for po studies (see Experimental Section and Supporting Information Table S2).

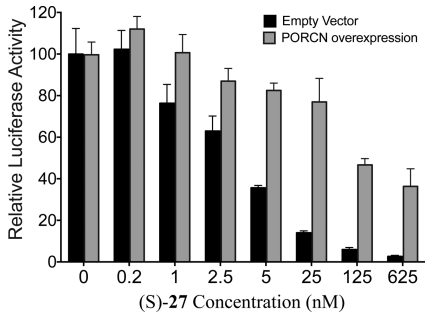

Figure 4. Effect of (*S*)-**27** on HT1080 cells treated with control plasmid in combination with Wnt/β-catenin reporter plasmid and Wnt3a (black bars) and effect of (*S*)-**27** on HT1080 cells treated with murine PORCN expression plasmid in combination with Wnt/β-catenin reporter plasmid and Wnt3a (gray bars).

Our approach to disrupt Wnt signaling involves blocking the secretion of Wnt proteins through inhibition of a key biosynthetic enzyme. High throughput screening of a β-catenin reporter assay followed by the removal of compounds that work downstream of the Wnt binding to Frizzled receptor and its co-receptors provided a hit that was shown to be a PORCN inhibitor. Classical SAR based cellular optimization led to a compound that inhibits Wnt secretion with nanomolar potency. Undesirable properties of the original hit, namely, limited solubility and Cyp inhibition, were removed through targeted modification of substituents and modulation of the overall lipophilicity, providing us with a PORCN inhibitor with excellent bioavailability and potent activity in a Wnt-driven murine tumor model. Finally we also discovered that enantiomeric PORCN inhibitors show very different activity in our reporter assay, suggesting that such compounds may be useful for mode of action studies on the PORCN *O*-acyltransferase.

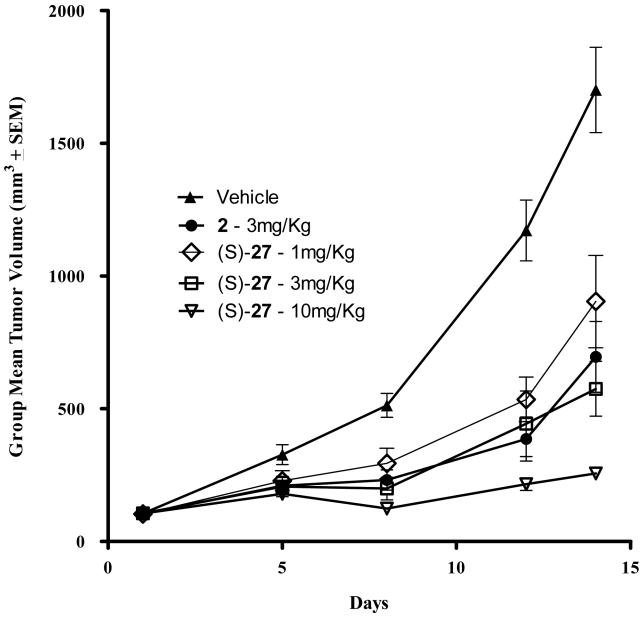

Figure 5. (*S*)-**27** inhibits the growth of MMTV-Wnt1 tumors. Tumor growth inhibition was 50% at 1 mg/kg, 71% at 3 mg/kg, and 91% at 10 mg/kg. Tumor growth inhibition compared with vehicle was statistically significant for all doses with a *p* value of <0.0001.

EXPERIMENTAL SECTION

General. All reagents were purchased from commercial sources and used as received. Reaction progress was monitored by TLC using Merck silica gel 60 F254 on glass plates with detection by UV at 254 nm. LC−MS analysis was carried out with Shimadzu LC-20AD and LCMS-2020 instruments. The column used was a Phenomenex Kinetex (2.6 μm, 50 mm × 2.10 mm). Proton nuclear magnetic resonance (^{1}H NMR) spectra were obtained using a Bruker Ultrashield 400 PLUS/R system, operating at 400 MHz. All resonance bands were referenced to tetramethylsilane (internal standard). Splitting patterns are indicated as follows: s, singlet; d, doublet; t, triplet; m, multiplet; br, broad peak. The compounds' purities were ≥95% determined by a VARIAN ProStar HPLC instrument.

Thermodynamic Solubility Studies. A 6 μL volume of 50 mM DMSO stock from the stock plate is added to the reaction deep well plate containing 600 μL of pH 7.4 or pH 4.0 pION buffer, mixed, and incubated for 18 h. The plate is sealed well during the incubation process. The test compound concentration is 500 μM. The DMSO content in the sample was 1.0%. At the end of the incubation period, 100 μL of sample from the storage plate is vacuum filtered using a filter plate. This step wets the filters, and the filtrate is discarded. Another 200 μL of the sample from the deep well plate is vacuum filtered using the same filter block but a clean filter plate. A 75 μL volume of the filtrate from the filter plate is transferred to a UV sample plate. A 75 μL volume of 1-propanol is added to this UV plate. The solution is mixed, and the spectrum is read using the UV spectrophotometer (Spectramax-Molecular Devices). The analysis is carried out by using pION μSOL EXPLORER software, version 3.3.

***N*-([1,1′-Biphenyl]-4-yl)-2-chloroacetamide (5).** To biphenyl-4-amine (500 mg, 2.95 mmol) in anhydrous DCM (15 mL) at 0 °C were added triethylamine (495 μL, 3.54 mmol) and 2-chloroacetyl chloride (282 μL, 1.418 mmol) dropwise. The reaction mixture was allowed to warm to room temperature and stirred for 2 h, and then it was diluted with H_2O (30 mL) and extracted with DCM (3 × 15 mL). The combined organic layer was dried over Na_2SO_4 and was concentrated under reduced pressure. The crude product **5** (600 mg, brown solid) was used without further purification. ^{1}H NMR (400 MHz, DMSO-d_6)

DOI: 10.1021/acs.jmedchem.5b00507
J. Med. Chem. XXXX, XXX, XXX−XXX

δ 10.38 (s, 1H), 7.70−7.63 (m, 6H), 7.46−7.42 (m, 2H), 7.35−7.31 (m, 1H), 4.27 (s, 2H); MS (ESI) m/z 246 $[C_{14}H_{12}ClNO + H]^+$.

General Synthesis Route for Compounds 6−10. To a solution of *N*-([1,1′-biphenyl]-4-yl)-2-chloroacetamide (0.316 mmol) and the respective phenols (0.316 mmol) in DMF (2 mL) was added K_2CO_3 (153 mg, 1.105 mmol). The solution was heated at 70 °C for 16 h, and then it was diluted with H_2O (25 mL) and extracted with EtOAc (3 × 25 mL). The combined organic layer was dried over Na_2SO_4 and was concentrated under reduced pressure to afford the crude product. The crude residue was purified by preparative HPLC (C18, eluent ACN, water, formic acid 0.1%) to afford the purified product.

2-(4-(1*H*-Imidazol-1-yl)phenoxy)-*N*-([1,1′-biphenyl]-4-yl)-acetamide (4). **4** was prepared according to the general procedure using commercially available 4-(1*H*-imidazol-1-yl)phenol and *N*-([1,1′-biphenyl]-4-yl)-2-chloroacetamide to give a white solid (yield, 31%). ^{1}H NMR (400 MHz, DMSO-d_6) δ 10.21 (s, 1H), 8.13 (s, 1H), 7.77−7.72 (m, 2H), 7.68−7.61 (m, 5H), 7.61−7.55 (m, 2H), 7.48−7.41 (m, 2H), 7.36−7.30 (m, 1H), 7.18−7.12 (m, 2H), 7.08 (s, 1H), 4.79 (s, 2H); MS (ESI) m/z 370 $[C_{23}H_{19}N_3O_2 + H]^+$. Melting point: 206−208 °C.

2-(4-(1*H*-Pyrrol-1-yl)phenoxy)-*N*-(biphenyl-4-yl)acetamide (6). **6** was prepared according to the general procedure using commercially available 4-(1*H*-pyrrol-1-yl)phenol and *N*-([1,1′-biphenyl]-4-yl)-2-chloroacetamide to give a beige solid (yield, 65%). ^{1}H NMR (400 MHz, DMSO-d_6) δ 10.20 (s, 1H), 7.76−7.74 (m, 2H), 7.66−7.64 (m, 4H), 7.52−7.42 (m, 4H), 7.35−7.31 (m, 1H), 7.25 (t, J = 2.0 Hz, 2H), 7.11−7.08 (m, 2H), 6.22 (t, J = 2.0 Hz, 2H), 4.75 (s, 2H); ^{13}C NMR (400 MHz, DMSO-d_6) δ 166.53, 155.45, 139.59, 137.80, 135.36, 134.14, 128.87, 127.06, 126.90, 126.25, 120.84, 120.04, 119.06, 115.62, 109.93, 67.48; MS (ESI) m/z 369 $[C_{24}H_{20}N_2O_2 + H]^+$. Melting point: 248−250 °C.

***N*-(Biphenyl-4-yl)-2-(4-(oxazol-5-yl)phenoxy)acetamide (7).** **7** was prepared according to the general procedure using commercially available 4-(oxazol-5-yl)phenol and *N*-([1,1′-biphenyl]-4-yl)-2-chloroacetamide to give an off-white solid (yield, 66%). ^{1}H NMR (400 MHz, DMSO-d_6) δ 10.20 (s, 1H), 8.38 (s, 1H), 7.77−7.72 (m, 2H), 7.72−7.67 (m, 2H), 7.67−7.62 (m, 4H), 7.55 (s, 1H), 7.48−7.41 (m, 2H), 7.36−7.30 (m, 1H), 7.16−7.10 (m, 2H), 4.79 (s, 2H); MS (ESI) m/z 371 $[C_{23}H_{18}N_2O_3 + H]^+$. Melting point: 244−246 °C.

2-(4-(1*H*-Pyrazol-3-yl)phenoxy)-*N*-(biphenyl-4-yl)acetamide (8). **8** was prepared according to the general procedure using commercially available 4-(1*H*-pyrazol-3-yl)phenol and *N*-([1,1′-biphenyl]-4-yl)-2-chloroacetamide to give an off-white solid (yield, 24%). ^{1}H NMR (400 MHz, DMSO-d_6) δ 10.42 (s, 1H), 9.44 (s, 1H), 7.76 (d, J = 2.4 Hz, 1H), 7.71−7.58 (m, 8H), 7.44 (t, J = 7.6 Hz, 2H), 7.32 (t, J = 7.6 Hz, 1H), 6.78−6.76 (m, 2H), 6.59 (d, J = 2.4 Hz, 1H), 5.04 (s, 2H); ^{13}C NMR (400 MHz, DMSO-d_6) δ 165.54, 156.87, 150.67, 139.50, 137.99, 135.17, 133.07, 128.79, 126.97, 126.94, 126.33, 126.16, 124.39, 119.48, 115.25, 101.75, 54.55; MS (ESI) m/z 370 $[C_{23}H_{19}N_3O_2 + H]^+$. Melting point: 213−215 °C.

***N*-(Biphenyl-4-yl)-2-(4-(2-methyl-1*H*-imidazol-1-yl)-phenoxy)acetamide (9).** **9** was prepared according to the general procedure using commercially available 4-(2-methyl-1*H*-imidazol-1-yl)phenol and *N*-([1,1′-biphenyl]-4-yl)-2-bromoacetamide to give a white solid (yield, 14%). ^{1}H NMR (400 MHz, DMSO-d_6) δ 10.23 (s, 1H), 7.76−7.74 (m, 2H), 7.66−7.64 (m, 4H), 7.46−7.31 (m, 5H), 7.20 (d, J = 1.6 Hz, 1H), 7.15−7.13 (m, 2H), 6.87 (d, J = 1.6 Hz, 1H), 4.80 (s, 2H), 2.24 (s, 3H); ^{13}C NMR (400 MHz, DMSO-d_6) δ 166.28, 157.19, 143.64, 139.52, 137.73, 135.31, 131.05, 128.80, 127.00, 126.87, 126.84, 126.51, 126.18, 120.93, 119.95, 115.30, 67.27, 13.31; MS (ESI) m/z 384 $[C_{24}H_{21}N_3O_2 + H]^+$. Melting point: 184−186 °C.

***N*-(Biphenyl-4-yl)-2-(4-(1-methyl-1*H*-pyrazol-5-yl)phenoxy)-acetamide (10).** **10** was prepared according to the general procedure using commercially available 4-(1-methyl-1*H*-pyrazol-5-yl)phenol and *N*-([1,1′-biphenyl]-4-yl)-2-chloroacetamide to give a white solid (yield, 91%). ^{1}H NMR (400 MHz, DMSO-d_6) δ 10.24 (bs, 1H), 7.78−7.73 (m, 2H), 7.68−7.62 (m, 4H), 7.52−7.41 (m, 5H), 7.37−7.30 (m, 1H), 7.15−7.10 (m, 2H), 6.33 (d, J = 1.6 Hz, 1H), 4.80 (s, 2H), 3.83 (s, 3H); ^{13}C NMR (400 MHz, DMSO-d_6): 166.39, 157.83, 142.32, 139.58, 137.80, 137.71, 135.34, 129.75, 128.84, 127.04, 126.88, 126.23, 123.22, 120.00, 114.93, 105.36, 67.17, 37.33; MS (ESI) m/z 384 $[C_{24}H_{21}N_3O_2 + H]^+$. Melting point: 166−168 °C.

2-((4-(1*H*-Imidazol-1-yl)phenyl)amino)-*N*-([1,1′-biphenyl]-4-yl)acetamide (11). **11** was synthesized according to the general procedure using 4-(1*H*-imidazol-1-yl)aniline and *N*-([1,1′-biphenyl]-4-yl)-2-chloroacetamide to give a white solid (yield, 45%). ^{1}H NMR (400 MHz, DMSO-d_6) δ 10.12 (s, 1H), 8.01 (s, 1H), 7.74−7.68 (m, 2H), 7.67−7.59 (m, 4H), 7.52 (s, 1H), 7.44 (t, J = 7.2 Hz, 2H), 7.37−7.29 (m, 3H), 7.04 (s, 1H), 6.72 (d, J = 8.8 Hz, 2H), 6.28 (t, J = 6.4 Hz, 1H), 3.94 (d, J = 6.0 Hz, 2H); MS (ESI) m/z 368.9 $[C_{23}H_{20}N_4O + H]^+$. Melting point: 230−232 °C.

(*S*)-2-(4-(1*H*-Imidazol-1-yl)phenoxy)-*N*-(biphenyl-4-yl)-propanamide ((*S*)-14). To a solution of (+)-*R*-ethyl lactate (3.12 mmol) in THF (250 mL) were added DIAD (3.44 mmol) and TPP (3.12 mmol) at room temperature, and the reaction mixture was stirred for 16 h. The reaction mixture was poured into ice−water (100 mL) and extracted with EtOAc (2 × 100 mL). The combined organics were washed with water, brine, dried over Na_2SO_4, filtered, and concentrated to give crude product. The crude product was washed with diethyl ether several times to remove TPPO. The combined organics were concentrated to give (*S*)-ethyl 2-(4-(1*H*-imidazol-1-yl)phenoxy)propanoate as a crude product. MS (ESI) m/z 261.12 $[C_{14}H_{16}N_2O_3 + H]^+$.

To a solution of (*S*)-ethyl 2-(4-(1*H*-imidazol-1-yl)phenoxy)-propanoate crude product (35.02 mmol) in 30 mL of THF−MeOH−H_2O was added LiOH (4.62 mmol) at rt. The reaction mixture was stirred at rt for 4 h. The reaction mixture was concentrated and diluted with water. The aqueous layer was acidified with sat. $KHSO_4$ solution and concentrated to give crude material which was extracted with 10% MeOH in $CHCl_3$ (3 × 100 mL). The combined organics were dried over Na_2SO_4, filtered, and concentrated to give (*S*)-2-(4-(1*H*-imidazol-1-yl)phenoxy)propanoic acid (*S*)-**13** (yield, 31%). ^{1}H NMR (400 MHz, DMSO-d_6) δ 8.5 (s, 1H), 8.06 (s, 1H), 7.58 (s, 1H), 7.42 (d, J = 9.2 Hz, 2H), 7.04 (s, 1H), 6.90 (d, J = 8.7 Hz, 2H), 4.30 (m, 1H) 2.50 (d, J = 1.8 Hz, 3H); MS (ESI) m/z 234.2 $[C_{12}H_{12}N_2O_3 + H]^+$.

(*S*)-**13** (0.65 mmol) was taken up in DMF (20 mL). DIPEA (1.96 mmol), HATU (1.30 mmol), and biphenyl-4-amine (0.65 mmol) were added to the reaction mixture. The reaction mixture was stirred for 16 h at room temperature. Upon completion, the reaction mixture was poured into ice−water (100 mL) and stirred for 30 min. The precipitated solid was filtered, washed with water, and dried to afford (*S*)-2-(4-(1*H*-imidazol-1-yl)phenoxy)-*N*-(biphenyl-4-yl)propanamide (*S*)-**14** as an off white solid (yield, 24%). ^{1}H NMR (400 MHz, DMSO-d_6) δ 10.27 (s, 1H), 8.13 (s, 1H), 7.74 (d, J = 8.4 Hz, 2H), 7.64 (m, 5H), 7.57 (d, J = 8.4 Hz, 2H), 7.44 (t, J = 7.25 Hz, 2H), 7.34−7.31 (m, 1H) 7.11 (d, J = 8.3 Hz, 3H), 4.97 (d, J = 6.6 Hz, 1H), 1.6 (d, J = 6.6 Hz, 3H); MS (ESI) m/z 384.14 $[C_{24}H_{21}N_3O_2 + H]^+$. Melting point: 238−240 °C.

(*R*)-2-(4-(1*H*-Imidazol-1-yl)phenoxy)-*N*-(biphenyl-4-yl)-propanamide ((*R*)-14). (*R*)-**14** was synthesized similarly to (*S*)-**14** using (−)-*S*-ethyl lactate as the starting material to afford an off white solid (yield, 28%). ^{1}H NMR (400 MHz, DMSO-d_6) δ 10.27 (s, 1H), 8.13 (s, 1H), 7.80−7.56 (m, 9H), 7.44 (t, J = 7.25 Hz, 2H), 7.34−7.32 (m, 1H) 7.11 (d, J = 8.3 Hz, 3H), 4.97 (d, J = 6.5 Hz, 1H), 1.6 (d, J = 5.7 Hz, 3H); MS (ESI) m/z 384.4 $[C_{24}H_{21}N_3O_2 + H]^+$. Melting point: 169−171 °C.

(*R*)-1-(4-Bromophenyl)pyrrolidine-2-carboxylic Acid ((*R*)-15). To a solution of 1,4-dibromobenzene (8.47 mmol) in 50 mL of DMF were added CuI (1.69 mmol), K_2CO_3 (25.43 mmol), and (*R*)-proline (9.32 mmol) at room temperature under argon. The reaction mixture was heated at 140 °C for 16 h. Upon completion, the reaction mixture was cooled to room temperature, poured into ice cold water (500 mL), and extracted with EtOAc (2 × 100 mL). The aqueous layer was acidified with sat. $KHSO_4$ solution and then extracted with EtOAc (2 × 100 mL). The combined organic layer was washed with water followed by brine, dried over Na_2SO_4, filtered, and concentrated under reduced pressure to afford (*R*)-1-(4-bromophenyl)pyrrolidine-2-carboxylic acid (*R*)-**15** (yield, 54%). ^{1}H NMR (400 MHz, DMSO-d_6) δ 12.90 (s, 1H), 7.95 (br s, 2H), 7.30 (br s, 2H), 4.01 (m, 1H),

DOI: 10.1021/acs.jmedchem.5b00507
J. Med. Chem. XXXX, XXX, XXX−XXX

3.32 (m, 2H), 2.05 (m, 4H); MS (ESI) m/z 271.8 $[C_{11}H_{12}BrNO_2 + H]^+$. MS (ESI) m/z 271.8 $[C_{11}H_{12}BrNO_2 + H]^+$.

(*S*)-1-(4-Bromophenyl)pyrrolidine-2-carboxylic Acid ((*S*)-15). (*S*)-**15** was synthesized similarly using 1,4-dibromobenzene and (*S*)-proline (yield, 54%). ^{1}H NMR (400 MHz, DMSO-d_6) δ 12.90 (s, 1H), 7.95 (br s, 2H), 7.30 (br s, 2H), 4.01 (m, 1H), 3.32 (m, 2H), 2.05 (m, 4H); MS (ESI) m/z 271.8 $[C_{11}H_{12}BrNO_2 + H]^+$.

(*R*)-*N*-(Biphenyl-4-yl)-1-(4-bromophenyl)pyrrolidine-2-carboxamide ((*R*)-16). To a solution of (*R*)-1-(4-bromophenyl)-pyrrolidine-2-carboxylic acid (*R*)-**15** (4.46 mmol) in DMF (25 mL) were added DIPEA (13.38 mmol), HATU (8.92 mmol), and biphenyl-4-amine (4.46 mmol), and the reaction mixture was stirred at room temperature for 16 h. After completion, the reaction mixture was poured into ice−water (100 mL) and stirred for 30 min. The precipitated solid was filtered and washed with water and dried to afford (*R*)-*N*-(biphenyl-4-yl)-1-(4-bromophenyl)pyrrolidine-2-carboxamide (*R*)-**16** (yield, 41%). ^{1}H NMR (400 MHz, DMSO-d_6) δ 10.08 (s, 1H), 7.70−7.68 (m, 2H), 7.64−7.60 (m, 4H), 7.44 (t, J = 7.7 Hz, 2H), 7.34−7.30 (m, 3H), 6.50−6.48 (d, J = 8.8 Hz, 2H), 4.23−4.20 (d, J = 8.4 Hz, 1 H), 3.60 (m, 1H), 3.32 (m, 1H), 1.40−1.25 (m, 1H), 2.08−2.00 (m, 3H); MS (ESI) m/z 421.09 $[C_{23}H_{21}BrN_2O + H]^+$.

(*S*)-*N*-(Biphenyl-4-yl)-1-(4-bromophenyl)pyrrolidine-2-carboxamide ((*S*)-16). (*S*)-**16** was synthesized similarly via amide coupling between (*S*)-1-(4-bromophenyl)pyrrolidine-2-carboxylic acid (*S*)-**15** and biphenyl-4-amine (yield, 54%). ^{1}H NMR (400 MHz, DMSO-d_6) δ 10.08 (s, 1H), 7.70−7.68 (m, 2H), 7.64−7.60 (m, 4H), 7.44 (t, J = 7.7 Hz, 2H), 7.34−7.30 (m, 3H), 6.50−6.48 (d, J = 8.8 Hz, 2H), 4.23−4.20 (d, J = 8.4 Hz, 1 H), 3.60 (m, 1H), 3.32 (m, 1H), 1.40−1.25 (m, 1H), 2.08−2.00 (m, 3H); MS (ESI) m/z 421.09 $[C_{23}H_{21}BrN_2O + H]^+$.

(*R*)-1-(4-(1*H*-Imidazol-1-yl)phenyl)-*N*-(biphenyl-4-yl)-pyrrolidine-2-carboxamide ((*R*)-17). Imidazole (1.227 mmol), (*R*)-*N*-(biphenyl-4-yl)-1-(4-bromophenyl)pyrrolidine-2-carboxamide (*R*)-**16** (0.356 mmol), CuI (0.036 mmol), L-proline (0.712 mmol), and Cs_2CO_3 (0.712 mmol) were dissolved in DMSO (2 mL). The reaction mixture was heated at 90 °C for 16 h. After completion, it was diluted with water (25 mL) and extracted with EtOAc (25 mL × 3). The combined organic extracts were concentrated and the residue was purified by preparative HPLC (C18, eluent ACN, water, formic acid 0.1%) to afford (*R*)-1-(4-(1*H*-imidazol-1-yl)phenyl)-*N*-(biphenyl-4-yl)pyrrolidine-2-carboxamide (*R*)-**17** as brown solid (yield, 29%). $[\alpha]^{20}_D$ 158 (c 0.1, MeOH). ^{1}H NMR (400 MHz, $CDCl_3$) δ 8.28 (s, 1H), 7.76 (br s, 1H), 7.59−7.53 (m, 6H), 7.41 (t, J = 7.2 Hz, 2H), 7.34−7.25 (m, 3H), 7.25−7.20 (m, 2H), 6.79 (d, J = 8.8 Hz, 2H), 4.15−4.12 (m, 1H), 3.84−3.80 (m, 1H), 3.37−3.30 (m, 1H), 2.44−2.39 (m, 2H), 2.16−2.08 (m, 2H); ^{13}C NMR (400 MHz, $CDCl_3$) δ 171.59, 146.95, 140.39, 137.69, 136.40, 128.79, 127.64, 127.22, 126.85, 123.44, 120.26, 114.14, 65.39, 50.34, 31.68, 24.35; MS (ESI) m/z 409 $[C_{26}H_{24}N_4O + H]^+$. Melting point: 182−184 °C.

(*S*)-1-(4-(1*H*-Imidazol-1-yl)phenyl)-*N*-(biphenyl-4-yl)-pyrrolidine-2-carboxamide ((*S*)-17). (*S*)-**17** was synthesized similarly via coupling between (*S*)-*N*-(biphenyl-4-yl)-1-(4-bromophenyl)pyrrolidine-2-carboxamide (*S*)-**16** and imidazole (yield, 41%; ee, 99.6%). $[\alpha]^{20}_D$ −181 (c 0.1, MeOH). ^{1}H NMR (400 MHz, $CDCl_3$) δ 8.28 (s, 1H), 7.76 (br s, 1H), 7.59−7.53 (m, 6H), 7.41 (t, J = 7.2 Hz, 2H), 7.34−7.25 (m, 3H), 7.25−7.20 (m, 2H), 6.79 (d, J = 8.8 Hz, 2H), 4.15−4.12 (m, 1H), 3.84−3.80 (m, 1H), 3.37−3.30 (m, 1H), 2.44−2.39 (m, 2H), 2.16−2.08 (m, 2H); ^{13}C NMR (400 MHz, $CDCl_3$) δ 171.59, 146.95, 140.39, 137.69, 136.40, 128.79, 127.64, 127.22, 126.85, 123.44, 120.26, 114.14, 65.39, 50.34, 31.68, 24.35; MS (ESI) m/z 409 $[C_{26}H_{24}N_4O + H]^+$. Melting point: 227−229 °C.

Ethyl 2-(4-Bromophenylamino)propanoate (18). To a solution of 4-bromoaniline (5.8 mmol) and ethyl 2-bromopropanoate (7 mmol) in acetonitrile (15 mL) was added K_2CO_3 (8.7 mmol). The solution was heated at 70 °C for 16 h. Solvent was then removed under reduced pressure, and then it was diluted with H_2O and extracted with EtOAc. The combined organic layer was dried over Na_2SO_4 and was concentrated under reduced pressure. The crude residue was purified by column chromatography to afford the desired product as yellow oil (yield, 57%). ^{1}H NMR (400 MHz, DMSO-d_6) δ 7.20 (d, J = 6.8 Hz, 2H), 6.50 (d, J = 6.8 Hz, 2H), 6.19 (d, J = 8.4 Hz, 1H), 4.11−3.99 (m, 3H), 1.36 (d, J = 6.8 Hz, 3H), 1.15 (t, J = 6.8 Hz, 3H); MS (ESI) m/z 204.9 $[C_{11}H_{14}BrNO_2 + H]^+$.

Ethyl 2-(4-(1*H*-Imidazol-1-yl)phenylamino)propanoate (19). Imidazole (2.9 mmol), ethyl 2-(4-bromophenylamino)propanoate **18** (1.5 mmol), CuI (0.15 mmol), L-proline (2.9 mmol), and Cs_2CO_3 (2.9 mmol) were dissolved in DMSO (3.5 mL). The reaction mixture was heated at 90 °C for 16 h, and then it was diluted with water and extracted with EtOAc. The combined organic extracts were concentrated and the residue was purified by column chromatography to afford the desired product as yellow oil (yield, 67%). ^{1}H NMR (400 MHz, DMSO-d_6) δ 7.98 (s, 1H), 7.50 (s, 1H), 7.30 (d, J = 6.8 Hz, 2H), 7.02 (s, 1H), 6.64 (d, J = 6.8 Hz, 2H), 6.20 (d, J = 8.4 Hz, 1H), 4.13−4.07 (m, 3H), 1.39 (d, J = 6.8 Hz, 3H), 1.17 (t, J = 7.2 Hz, 3H); MS (ESI) m/z 260 $[C_{14}H_{17}N_3O_2 + H]^+$.

2-(4-(1*H*-Imidazol-1-yl)phenylamino)-*N*-(5-phenylpyridin-2-yl)propanamide (20). To ethyl 2-(4-(1*H*-imidazol-1-yl)-phenylamino)propanoate **19** 0.96 mmol) in H_2O (1 mL) and THF (1 mL) was added lithium hydroxide (1.9 mmol). The reaction mixture was stirred at room temperature for 1 h and was then acidified using 1 M HCl solution. Solvent was then evaporated in vacuo, and the crude residue was used without further purification. ^{1}H NMR (400 MHz, DMSO-d_6) δ 9.54 (s, 1H), 8.11 (s, 1H), 7.85 (s, 1H), 7.47 (d, J = 9.2 Hz, 2H), 7.72 (d, J = 8.8 Hz, 2H), 4.06 (q, J = 7.2 Hz, 1H), 1.40 (d, J = 6.8 Hz, 3H); MS (ESI) m/z 232 $[C_{12}H_{13}N_3O_2 + H]^+$.

To the crude material (0.48 mmol) in DMF (2.5 mL) were added HATU (0.72 mmol) and *N*-methylmorpholine (1.92 mmol). The reaction mixture was stirred at room temperature under inert atmosphere for 1 h, followed by the addition of 5-phenylpyridin-2-amine (0.72 mmol). The reaction mixture was left to stir for 16 h, and then it was diluted with H_2O and extracted with EtOAc. The combined organic layer was dried over Na_2SO_4 and was concentrated under reduced pressure. The crude residue was purified by column chromatography to afford racemate compound **20** as an off-white solid (yield, 10%). Isomers were separated by chiral HPLC (CHIRALPAK ASH column; hexane/EtOH/isopropyamine 20:80:0.1) to afford the required compound (*S*)-**20** (yield, 35%) and (*R*)-**20** (yield, 32%).

(*S*)-**20**. $[\alpha]^{20}_D$ −61.6 (c 0.26, MeOH). ^{1}H NMR (400 MHz, DMSO-d_6) δ 10.59 (s, 1H), 8.64 (d, J = 2.0 Hz, 1H), 8.17−8.15 (m, 1H), 8.10−8.07 (m, 1H), 7.97 (s, 1H), 7.70−7.68 (m, 2H), 7.50−7.45 (m, 3H), 7.40−7.31 (m, 3H), 7.00 (s, 1H), 6.73 (d, J = 8.8 Hz, 2H), 6.25 (d, J = 8.4 Hz, 1H), 4.31−4.23 (m, 1H), 1.44 (d, J = 6.8 Hz, 3H); MS (ESI) m/z 384 $[C_{23}H_{21}N_5O + H]^+$. Melting point: 88−90 °C.

(*R*)-**20**. $[\alpha]^{20}_D$ 78.2 (c 0.26, MeOH).^{1}H NMR (400 MHz, DMSO-d_6) δ 10.59 (s, 1H), 8.64 (d, J = 2.0 Hz, 1H), 8.17−8.15 (m, 1H), 8.10−8.07 (m, 1H), 7.97 (s, 1H), 7.70−7.68 (m, 2H), 7.50−7.45 (m, 3H), 7.40−7.31 (m, 3H), 7.00 (s, 1H), 6.73 (d, J = 8.8 Hz, 2H), 6.25 (d, J = 8.4 Hz, 1H), 4.31−4.23 (m, 1H), 1.44 (d, J = 6.8 Hz, 3H); MS (ESI) m/z 384 $[C_{23}H_{21}N_5O + H]^+$. Melting point: 98−100 °C.

2-(1-Methyl-1*H*-pyrazol-5-yl)-5-nitropyridine (21). To a well stirred solution of 2-bromo-5-nitropyridine (4.9 mmol) in dioxane−water (4:1, 50 mL) were added K_3PO_4 (9.8 mmol), 1-methyl-5-(4,4,5,5-tetramethyl-1,3,2-dioxaborolan-2-yl)-1*H*-pyrazole (4.9 mmol), and $Pd(PPh_3)_4$ (0.25 mmol) under Ar, and the reaction mixture was heated at 100 °C for 16 h. The reaction mixture was evaporated under reduced pressure. The residue was poured into ice−water, and the compound was extracted with EtOAc (3 × 50 mL). The combined organic layer was washed with ice−water, brine, dried over anhydrous Na_2SO_4, filtered, and concentrated under reduced pressure. The crude material was purified by column chromatography (silica gel, eluent EtOAc/hexane 25:75) to afford 2-(1-methyl-1*H*-pyrazol-5-yl)-5-nitropyridine **21** (yield, 85%). ^{1}H NMR (400 MHz, DMSO-d_6) δ 9.46 (d, J = 2.8 Hz, 1H), 8.67 (dd, J = 2.4, 8.8 Hz, 1H), 8.12 (d, J = 8.8 Hz, 1H), 7.59 (d, J = 2 Hz, 1H), 9.09 (d, J = 2 Hz, 1H), 4.21 (s, 3H); MS (ESI) m/z 204.9 $[C_9H_8N_4O_2 + H]^+$.

6-(1-Methyl-1*H*-pyrazol-5-yl)pyridin-3-amine (22). To a stirred solution of 2-(1-methyl-1*H*-pyrazol-5-yl)-5-nitropyridine **21** (2.1 mmol) in EtOAc (20 mL) was added 10% Pd/C (20% by wt), and the mixture was hydrogenated under H_2 (balloon) at room temperature for 12 h. After completion, the reaction mixture was

DOI: 10.1021/acs.jmedchem.5b00507
J. Med. Chem. XXXX, XXX, XXX−XXX

filtered through Celite pad and washed with EtOAc. Filtrate was concentrated under reduced pressure to afford 6-(1-methyl-1*H*-pyrazol-5-yl)pyridin-3-amine **22** as a yellow solid (yield, 96%). ^{1}H NMR (400 MHz, DMSO-d_6) δ 8.01 (d, J = 1.6 Hz, 1H), 7.39 (m, 2H), 6.99 (m, 1H), 6.47 (s, 1H), 5.58 (s, 2H), 4.03 (s, 3H); MS (ESI) m/z 175.1 $[C_9H_{10}N_4 + H]^+$.

Ethyl 2-(6-(1-Methyl-1*H*-pyrazol-5-yl)pyridin-3-ylamino)-propanoate (23). To a stirred solution of 6-(1-methyl-1*H*-pyrazol-5-yl)pyridin-3-amine **22** (2 mmol) in acetonitrile (20 mL) was added NaOAc (6 mmol) and ethyl bromopropionate (2 mmol), and the reaction mixture was heated to reflux for 48 h. The reaction mixture was concentrated under reduced pressure and the crude material was purified by column chromatography (silica gel, eluent EtOAc/hexane 20:80) to afford ethyl 2-(6-(1-methyl-1*H*-pyrazol-5-yl)pyridin-3-ylamino)propanoate **23** as a colorless liquid (yield, 45%). ^{1}H NMR (400 MHz, DMSO-d_6) δ 8.04 (d, J = 2.8 Hz, 1H), 7.48 (d, J = 8.8 Hz, 1H), 7.38 (d, J = 2.4 Hz, 1H), 6.98 (dd, J = 2.4, 8.8 Hz, 1H), 6.54 (d, J = 8.4 Hz, 1H), 6.51 (s, 1H), 4.21 (q, J = 6.8 Hz, 1H), 4.14 (q, J = 7.6 Hz, 2H), 4.04 (s, 3H), 1.41 (d, J = 6.8 Hz, 3H), 1.18 (t, J = 7.6 Hz, 3H); MS (ESI) m/z 275.2 $[C_{14}H_{18}N_4O_2 + H]^+$.

2-(6-(1-Methyl-1*H*-pyrazol-5-yl)pyridin-3-ylamino)propanoic Acid (24). To a stirred solution of ethyl 2-(6-(1-methyl-1*H*-pyrazol-5-yl)pyridin-3-ylamino)propanoate **23** (1 mmol) in THF−H_2O−MeOH (1:1:1) (15 mL) was added LiOH (2 mmol), and the reaction mixture was stirred at room temperature for 2 h. After completion, the volatiles were removed under reduced pressure and the residue was acidified with aq $KHSO_4$ and extracted into EtOAc. The combined organic layer was washed with brine, dried over anhydrous Na_2SO_4, filtered, and concentrated under reduced pressure to afford 2-(6-(1-methyl-1*H*-pyrazol-5-yl)pyridin-3-ylamino)propanoic acid **24** (yield, 89%). ^{1}H NMR (400 MHz, DMSO-d_6) δ 8.05 (d, J = 2.8 Hz, 1H), 7.61 (d, J = 8.8 Hz, 1H), 7.45 (s, 1H), 7.21 (br s, 1H), 6.56 (br s, 1H), 4.44 (br s, 1H), 4.29 (m, 1H), 4.17 (m, 1H), 3.99 (s, 3H), 1.40 (d, J = 7.2 Hz, 3H); MS (ESI) m/z 247.2 $[C_{12}H_{14}N_4O_2 + H]^+$.

***N*-(2,3′-Bipyridin-5-yl)-2-(6-(1-methyl-1*H*-pyrazol-5-yl)-pyridin-3-ylamino)propanamide ((*S*)-25).** To a stirred solution of 2-(6-(1-methyl-1*H*-pyrazol-5-yl)pyridin-3-ylamino)propanoic acid **24** (0.8 mmol) in DMF (5 mL) were added HATU (1.2 mmol), 2,3′-bipyridin-5-amine (0.8 mmol), and DIPEA (1.6 mmol). The reaction mixture was stirred at room temperature for 16 h. After completion, the reaction mixture was poured into ice−water and the compound was extracted with EtOAc (3 × 50 mL). The combined organic layer was washed with ice−water, brine, dried over anhydrous Na_2SO_4, filtered, and concentrated under reduced pressure. The crude material was purified by column chromatography (silica gel, eluent MeOH/chloroform 5:95) to afford *N*-(2,3′-bipyridin-5-yl)-2-(6-(1-methyl-1*H*-pyrazol-5-yl)pyridin-3-ylamino)propanamide **25** racemate. Isomers were separated by chiral HPLC to afford the required compound (*S*)-**25** (yield, 10%). $[\alpha]^{20}_D$ −51.4 (*c* 1.19, $CHCl_3$). ^{1}H NMR (400 MHz, $CDCl_3$) δ: 10.52 (s, 1H), 9.21 (d, J = 1.8 Hz, 1H), 8.90 (d, J = 2.2 Hz, 1H), 8.59 (dd, J = 1.3 Hz, 4.8 Hz, 1H), 8.37 (dt, J = 1.7, 8.0 Hz, 1H), 8.22 (dd, J = 2.6, 8.6 Hz, 1H), 8.11 (d, J = 2.6 Hz, 1H), 8.03 (d, J = 8.8 Hz, 1H), 7.55−7.45 (m, 2H), 7.37 (d, J = 1.7 Hz, 1H), 7.04 (dd. J = 2.6, 8.30 Hz, 1H), 6.60 (d, J = 7.5 Hz, 1H), 6.50 (d, J = 1.8 Hz, 1H), 4.22 (t, J = 7.0 Hz, 1H), 4.03 (s, 3H), 1.49 (d, J = 6.6 Hz, 3H); MS (ESI) m/z 400.25 $[C_{22}H_{21}N_7O + H]^+$. Melting point: 98−100 °C.

2-(6-(1-Methyl-1*H*-pyrazol-5-yl)pyridin-3-ylamino)-*N*-(5-phenylpyridin-2-yl)propanamide ((*S*)-26). To a stirred solution of 2-(6-(1-methyl-1*H*-pyrazol-5-yl)pyridin-3-ylamino)propanoic acid **24** (1 mmol) in DMF (5 mL) were added HATU (2 mmol), 2-amino-5-phenylpyridine 1-oxide (1 mmol), and DIPEA (3 mmol). The reaction mixture was stirred at room temperature for 16 h. The reaction mixture was poured into ice−water and extracted with EtOAc (3 × 10 mL). The combined organic layers were washed with water and brine solution, dried over anhydrous Na_2SO_4, filtered, and concentrated under reduced pressure to afford 2-(2-(6-(1-methyl-1*H*-pyrazol-5-yl)pyridin-3-ylamino)propanamido)-5-phenylpyridine 1-oxide as an off-white solid.

To a stirred solution of 2-(2-(6-(1-methyl-1*H*-pyrazol-5-yl)pyridin-3-ylamino)propanamido)-5-phenylpyridine 1-oxide (1.44 mmol) was added iron (7.2 mmol) in AcOH (1 mL), and the reaction mixture was stirred at reflux for 2 h. The reaction mixture was concentrated under reduced pressure and basified with sat. $NaHCO_3$ and extracted with EtOAc (3 × 10 mL) and purified by column chromatography (silica gel, eluent MeOH/DCM 5:95) to afford 2-(6-(1-methyl-1*H*-pyrazol-5-yl)pyridin-3-ylamino)-*N*-(5-phenylpyridin-2-yl)propanamide **26** racemate as an off-white solid. Chiral separation (CHIRALPAK IA column; hexane/EtOH/TFA 20:80:0.1) gave the desired compound (*S*)-**26** (yield, 2%, chiral HPLC 99%). $[\alpha]^{20}_D$ −72.6 (*c* 0.5, $CHCl_3$). ^{1}H NMR (400 MHz, DMSO-d_6) δ 9.02 (s, 1H), 8.47 (s, 1H), 8.36 (d, J = 8.4 Hz, 1H), 8.19 (s, 1H), 7.95 (d, J = 10.8 Hz, 1H), 7.54 (d, J = 7.6 Hz, 2H), 7.48−7.36 (m, 5H), 7.0 (d, J = 11.2 Hz, 1H), 6.43 (s, 1H), 4.24 (s, 1H), 4.14 (s, 1H), 4.01 (s, 3H), 1.70 (d, J = 7.2 Hz, 3H,); MS (ESI) m/z 399.25 $[C_{23}H_{22}N_6O + H]^+$. Melting point: 82−84 °C.

***N*-(3,3′-Bipyridin-6-yl)-2-(6-(1-methyl-1*H*-pyrazol-5-yl)-pyridin-3-ylamino)propanamide ((*S*)-27).** To a stirred solution of 2-(6-(1-methyl-1*H*-pyrazol-5-yl)pyridin-3-ylamino)propanoic acid **24** (4.1 mmol) in DMF (5 mL) were added HATU (8.1 mmol), 2-amino-5-bromopyridine 1-oxide (4.1 mmol), and DIPEA (12.2 mmol). The reaction mixture was stirred at room temperature for 16 h. The reaction mixture was poured into ice−water and extracted with EtOAc (3 × 10 mL). The combined organic layers were washed with water and brine solution, dried over anhydrous Na_2SO_4, filtered, and concentrated under reduced pressure to afford 5-bromo-2-(2-(6-(1-methyl-1*H*-pyrazol-5-yl)pyridin-3-ylamino)propanamido)pyridine 1-oxide as a liquid (yield, 60%).

To a stirred solution of 5-bromo-2-(2-(6-(1-methyl-1*H*-pyrazol-5-yl)pyridin-3-ylamino)propanamido)pyridine 1-oxide (2.4 mmol) was added iron (12 mmol) in AcOH (5 mL), and the reaction mixture was stirred at reflux for 2 h. The reaction mixture was concentrated under reduced pressure, basified with sat. $NaHCO_3$, extracted with EtOAc (3 × 10 mL), and purified by column chromatography (silica gel, eluent CH_2Cl_2/CH_3OH 95:5) to afford *N*-(5-bromopyridin-2-yl)-2-(6-(1-methyl-1*H*-pyrazol-5-yl)pyridin-3-ylamino)propanamide as an off-white solid (yield, 64%).

To a well stirred solution of *N*-(5-bromopyridin-2-yl)-2-(6-(1-methyl-1*H*-pyrazol-5-yl)pyridin-3-ylamino)propanamide (1.4 mmol) in dioxane−water (4:1, 10 mL) were added K_3PO_4 (2.74 mmol), pyridine-3-boronic acid (1.4 mmol), and Pd(dppf)Cl_2·DCM (5 mol %) under Ar, and the reaction mixture was heated at 100 °C for 16 h. The reaction mixture was evaporated under reduced pressure. The residue was poured into ice−water, and the compound was extracted with EtOAc (3 × 50 mL). The combined organic layer was washed with ice−water, brine, dried over anhydrous Na_2SO_4, filtered, and concentrated under reduced pressure. The crude material was purified prep-HPLC to afford *N*-(3,3′-bipyridin-6-yl)-2-(6-(1-methyl-1*H*-pyrazol-5-yl)pyridin-3-ylamino)propanamide **27** racemate. Chiral separation (CHIRALCEL OJ-H column; hexane/EtOH/IPA 50:50:0.1) gave (*S*)-**27** as an off white solid (yield, 11%). $[\alpha]^{20}_D$ −72.5 (*c* 0.5, $CHCl_3$). ^{1}H NMR (400 MHz, DMSO-d_6) δ 10.79 (s, 1H), 8.93 (s, 1H), 8.74 (s, 1H), 8.58 (d, J = 4.8 Hz, 1H), 8.20 (s, 2H), 8.12 (m, 2H), 7.50 (m, 2H), 7.36 (s, 1H), 7.06 (d, J = 8.8 Hz, 1H), 6.54 (d, J = 8.4 Hz, 1H), 6.49 (s, 1H), 4.28 (t, J = 6.8 Hz, 1H), 4.03 (s, 3H), 1.48 (d, J = 6.8 Hz, 3H); ^{13}C NMR (400 MHz, $CDCl_3$) δ 172.36, 150.78, 148.86, 147.64, 146.17, 141.48, 141.42, 141.26, 138.18, 137.19, 135.84, 134.58, 133.30, 130.16, 124.09, 123.74, 120.63, 114.20, 105.61, 55.87, 39.17, 19.74; MS (ESI) m/z 400.47 $[C_{22}H_{21}N_7O + H]^+$. Melting point: 98−100 °C.

STF3A Reporter Assay. HEK293-STF3A cells and the assay used to determine the IC_{50} of the compounds were described by Coombs and co-workers.[15] 2 × 10^4 STF3A cells were seeded in each well of a 96-well plate (Greiner) and incubated overnight at 37 °C. An amount of 25 μL of serially diluted compound was added to the cells to give final concentrations of 50 μM to 1.5 nM. After 1 day of treatment, 100 μL of Steady-Glo luciferase assay reagent (Promega) was added to each well and incubated for 10 min at room temperature. Luminescence was measured using the Tecan Safire2 microplate reader.

DOI: 10.1021/acs.jmedchem.5b00507
J. Med. Chem. XXXX, XXX, XXX−XXX

STF/Wnt3A Conditioned Medium Assay. For this assay HEK293-STF cells that do not express Wnt3A were used. To make Wnt3A conditioned medium, mouse L-Wnt3A cells were cultured in three T-175 flasks at 3×10^4 cells/mL in 30 mL culture medium per flask. After 4 days of incubation, the Wnt3A-conditioned medium was harvested. An amount of 2×10^4 HEK293-STF cells in 25 μL of culture medium was added to each well of a 96 well plate (Greiner). 25 μL of serially diluted compound was added. After 4 h of incubation, 100 μL of Wnt-3A-conditioned medium was added to the cells. The final concentration of compound ranged from 33 μM to 1 nM. After incubation for 1 day at 37 °C, 100 μL of Steady-Glo luciferase assay reagent (Promega) was added to each well and incubated for 10 min at room temperature. Luminescence was measured using the Tecan Safire2 microplate reader.

Cell Viability Assay. 5000 cells in 75 μL of culture medium were seeded in each well of black 96-well plates (Greiner no. 655090) and incubated overnight at 37 °C. 25 μL of serially diluted compound was added to the cells giving a final concentration of 50 μM to 1.5 nM. After 1 day of treatment, 100 μL of CellTiter-Glo luminescent cell viability assay reagent (no. G7571, Promega) was added to each well and incubated for 10 min at room temperature. Luminescence was measured using Tecan Safire2 microplate reader.

Wnt3A Palmitoleation Assay. The assay used to determine the inhibition of the palmitoleation of Wnts by the compounds was described by Yap et al.[19] 3×10^6 HeLa cells were seeded in a 10 cm culture dish and incubated at 37 °C overnight. The cells were transfected with 5 μg of pcDNA3.2/V5-Wnt3a vector[18] to overexpress V5-tagged Wnt3a. After 6 h, the cells were washed with PBS and treated with 100 μM ω-alkynyl palmitate in medium with 5% fatty acid free BSA. 100 nM compound or DMSO was added, and the cells were incubated overnight at 37 °C. The cells were lysed, and 600 μg of cell lysate was collected and incubated with anti-V5 antibody (Invitrogen) followed by the pull down of V5-Wnt3a with the addition of protein A/G agarose beads (Thermo Scientific). The pulled down lysates containing V5-Wnt3a was click-reacted with biotin azide (Invitrogen). The biotin-labeled protein lysate was then separated by SDS−PAGE and transferred to a nitrocellulose membrane. The membrane was incubated with primary anti-V5 antibody, followed by secondary anti-mouse Dylight 680 (Thermo scientific) to detect V5-Wnt3a. The membrane was then incubated with streptavidin-Dylight 800 (Thermo Scientific) to detect biotin labeled Wnt3a. The signals were captured on the Odyssey CLx infrared imaging system (LI-COR Bioscience).

PORCN Overexpression Assay. The human fibrosarcoma cell line HT1080 (ATCC cat. no. CCL121) was maintained in DMEM (Nacali Tesque, Japan) containing 4.5 g/L glucose, penicillin/streptomycin, 10% FBS, and 1 mM sodium pyruvate in a humidified 37 °C atmosphere. The HT1080 cells were seeded at 150 000 per well in 24-well culture dishes 1 day prior to transfection. The cells were then transfected with either control plasmid or murine PORCN expression plasmids (100 ng) in combination with Wnt/β-catenin reporter plasmid (550 ng) and Wnt3a (50 ng) using Lipofectamine 2000 (Invitrogen/LifeTechnologies). The cells were treated with serially diluted (*S*)-**27** in concentrations from 625 to 0.2 nM at a final DMSO concentration of 0.1%. The activation of the β-catenin reporter gene activity was measured in 50 μL of cell lysate 24 h post-transfection, using the luciferase assay kit (Promega) according to the manufacturer's recommendations, on a Tecan Infinite M200 plate reader. Luminescence was read with no attenuation and an integration time of 1000 ms.

In Vivo Efficacy Studies. In vivo antitumor efficacy study was conducted at Charles River Discovery Research Services North Carolina, USA. The experimental protocols were in compliance with the recommendations of the Guide for Care and Use of Laboratory Animals.

The primary mammary tumors (MMTV-Wnt1) provided by Experimental Therapeutics Centre, Singapore, were passaged in female NCr nude mice prior to implantation. The tumor fragment utilized in this experiment originated from working tumor bank no. 947 R75. Each test mouse received a 3 mm^3 MMTV-Wnt1 fragment implanted in the mammary fat pad number 4. The growth of tumors was monitored using calipers. Fourteen days after tumor implantation (designated as day 1 of the study), mice bearing established orthotopic MMTV-Wnt1 tumors were selected and randomly distributed into five groups. Each group contained 10 mice. The group mean tumor volume ranged from 103 to 107 mm^3. After randomization, mice bearing established orthotopic MMTV-Wnt1 tumors received vehicle (50% polyethylene glycol (PEG) 400 in deionized water), **2**, or (*S*)-**27** once daily for 14 days via oral gavage. The volume of oral administration was 10 mL/kg. The dosing level for **2** was 3 mg/kg, and the dosing levels for (*S*)-**27** were 1, 3, and 10 mg/kg. The end point used to measure the response of the MMTV-Wnt1 tumors after compound treatment was tumor growth inhibition at day 14 and was expressed as % TGI and T/C ratio. The percentage of tumor growth inhibition (%TGI) was calculated as follows:

$$\%\,\mathrm{TGI} = \frac{C_{\mathrm{day}\,a} - T_{\mathrm{day}\,a}}{C_{\mathrm{day}\,a} - C_{\mathrm{day}\,1}} \times 100$$

where $C_{\mathrm{day}\,a}$ is the mean tumor volume of the vehicle control group at the indicated day a, $T_{\mathrm{day}\,a}$ is the mean tumor volume of the group treated with the test compound at the indicated day a, and $C_{\mathrm{day}\,1}$ is the mean tumor volume of the vehicle control group at day 1. The T/C ratio was calculated as follows:

$$\frac{T}{C} = \frac{T_{\mathrm{day}\,a}}{C_{\mathrm{day}\,a}}$$

One-way ANOVA followed by Dunnett's multiple comparison test was used to determine statistically significant differences between the tumor volumes of the vehicle control group and the tumor volumes of the group treated with different dosing regimens of **2** and (*S*)-**27**.

■ ASSOCIATED CONTENT

Ⓢ Supporting Information

Schematic representation of HTS strategy; ^{1}H and ^{13}C NMR data for (*S*)-**27**; solubility for compounds **4**, **6**−**11**, (*S*)-**14**, and (*S*)-**17**, and (S)-**20**; graphs for in vivo pharmacokinetics; tabulated results for the MMTV-Wnt1 in vivo model for compound (*S*)-**27**; mouse body weight for efficacy results; csv file containing molecular formula strings. The Supporting Information is available free of charge on the ACS Publications website at DOI: 10.1021/acs.jmedchem.5b00507.

■ AUTHOR INFORMATION

Corresponding Author

*E-mail: syho@etc.a-star.edu.sg. Telephone: +65 6407 0670.

Present Address

§A.J.D.: GVK Biosciences Private Limited, Plot No. 28 A, IDA Nacharam, Hyderabad, 500076, India.

Author Contributions

The manuscript was written through contributions of all authors. All authors have given approval to the final version of the manuscript.

Notes

The authors declare the following competing financial interest(s): All authors are current or former employees of the Experimental Therapeutics Centre or Duke-NUS Graduate Medical School Singapore. Both institutes have a commercial interest in the development of Wnt secretion inhibitors.

■ ACKNOWLEDGMENTS

We acknowledge the technical assistance provided by members of Experimental Therapeutics Centre including Jeff Hill, Shermaine Q. Y. Lim, and Sifang Wang, and we acknowledge Justina Fulwood and Horst Flotow for performing the high throughput screening of our compound library. This work was

DOI: 10.1021/acs.jmedchem.5b00507
J. Med. Chem. XXXX, XXX, XXX−XXX

supported in part by the Singapore Translational Research Investigator Award (D.M.V.), funded by the National Research Foundation and the National Medical Research Council of Singapore.

■ ABBREVIATIONS USED

Cyp, cytochrome P450 enzyme; ER, endoplasmic reticulum; HTS, high throughput screening; MMTV, mouse mammary tumor virus; PORCN, porcupine Wnt *O*-acyltransferase; SAR, structure−activity relationship; STF, super top flash

■ REFERENCES

(1) (a) Logan, C. Y.; Nusse, R. The Wnt signaling pathway in development and disease. *Annu. Rev. Cell Dev. Biol.* **2004**, *20*, 781−810. (b) van Amerongen, R.; Nusse, R. Towards an integrated view of Wnt signaling in development. *Development* **2009**, *136* (19), 3205−3214.

(2) Anastas, J. N.; Moon, R. T. Wnt signalling pathways as therapeutic targets in cancer. *Nat. Rev. Cancer* **2012**, *13* (1), 11−26.

(3) Ouyang, H.; Zhuo, Y.; Zhang, K. Wnt signaling in stem cell differentiation and tumor formation. *J. Clin. Invest.* **2013**, *123* (4), 1422−1424.

(4) Pecina-Slaus, N. Wnt signal transduction pathway and apoptosis: a review. *Cancer Cell Int.* **2010**, *10*, 22.

(5) Montcouquiol, M.; Crenshaw, E. B., 3rd; Kelley, M. W. Noncanonical Wnt signaling and neural polarity. *Annu. Rev. Neurosci.* **2006**, *29*, 363−386.

(6) Kahn, M. Can we safely target the Wnt pathway? Nature reviews. *Nat. Rev. Drug Discovery* **2014**, *13* (7), 513−532.

(7) Kurayoshi, M.; Yamamoto, H.; Izumi, S.; Kikuchi, A. Post-translational palmitoylation and glycosylation of Wnt-5a are necessary for its signalling. *Biochem. J.* **2007**, *402* (3), 515−523.

(8) Gao, X.; Hannoush, R. N. Single-cell imaging of Wnt palmitoylation by the acyltransferase porcupine. *Nat. Chem. Biol.* **2013**, *10* (1), 61−68.

(9) Herr, P.; Hausmann, G.; Basler, K. Wnt secretion and signalling in human disease. *Trends Mol. Med.* **2012**, *18* (8), 483−493.

(10) Brunner, E.; Peter, O.; Schweizer, L.; Basler, K. Pangolin encodes a Lef-1 homologue that acts downstream of armadillo to transduce the wingless signal in drosophila. *Nature* **1997**, *385* (6619), 829−833.

(11) Proffitt, K. D.; Madan, B.; Ke, Z.; Pendharkar, V.; Ding, L.; Lee, M. A.; Hannoush, R. N.; Virshup, D. M. Pharmacological inhibition of the Wnt acyltransferase PORCN prevents growth of Wnt-driven mammary cancer. *Cancer Res.* **2013**, *73* (2), 502−507.

(12) Chen, B.; Dodge, M. E.; Tang, W.; Lu, J.; Ma, Z.; Fan, C. W.; Wei, S.; Hao, W.; Kilgore, J.; Williams, N. S.; Roth, M. G.; Amatruda, J. F.; Chen, C.; Lum, L. Small molecule-mediated disruption of Wnt-dependent signaling in tissue regeneration and cancer. *Nat. Chem. Biol.* **2009**, *5* (2), 100−107.

(13) Wang, X.; Moon, J.; Dodge, M. E.; Pan, X.; Zhang, L.; Hanson, J. M.; Tuladhar, R.; Ma, Z.; Shi, H.; Williams, N. S.; Amatruda, J. F.; Carroll, T. J.; Lum, L.; Chen, C. The development of highly potent inhibitors for porcupine. *J. Med. Chem.* **2013**, *56* (6), 2700−2704.

(14) Liu, J.; Pan, S.; Hsieh, M. H.; Ng, N.; Sun, F.; Wang, T.; Kasibhatla, S.; Schuller, A. G.; Li, A. G.; Cheng, D.; Li, J.; Tompkins, C.; Pferdekamper, A.; Steffy, A.; Cheng, J.; Kowal, C.; Phung, V.; Guo, G.; Wang, Y.; Graham, M. P.; Flynn, S.; Brenner, J. C.; Li, C.; Villarroel, M. C.; Schultz, P. G.; Wu, X.; McNamara, P.; Sellers, W. R.; Petruzzelli, L.; Boral, A. L.; Seidel, H. M.; McLaughlin, M. E.; Che, J.; Carey, T. E.; Vanasse, G.; Harris, J. L. Targeting Wnt-driven cancer through the inhibition of porcupine by LGK974. *Proc. Natl. Acad. Sci. U. S. A.* **2013**, *110* (50), 20224−20229.

(15) Coombs, G. S.; Yu, J.; Canning, C. A.; Veltri, C. A.; Covey, T. M.; Cheong, J. K.; Utomo, V.; Banerjee, N.; Zhang, Z. H.; Jadulco, R. C.; Concepcion, G. P.; Bugni, T. S.; Harper, M. K.; Mihalek, I.; Jones, C. M.; Ireland, C. M.; Virshup, D. M. WLS-dependent secretion of Wnt3A requires Ser209 acylation and vacuolar acidification. *J. Cell Sci.* **2010**, *123* (19), 3357−3367.

(16) Willert, K.; Brown, J. D.; Danenberg, E.; Duncan, A. W.; Weissman, I. L.; Reya, T.; Yates, J. R., 3rd; Nusse, R. Wnt proteins are lipid-modified and can act as stem cell growth factors. *Nature* **2003**, *423* (6938), 448−452.

(17) Poulsen, A.; Ho, S. Y.; Wang, W.; Alam, J.; Jeyaraj, D. A.; Ang, S. H.; Tan, E. S.; Lin, G. R.; Cheong, V. W.; Ke, Z.; Lee, M. A.; Keller, T. H. A pharmacophore model for Wnt/porcupine inhibitors and its use for drug design. *J. Chem. Inf. Model.* **2015**, DOI: 10.1021/acs.jcim.5b00159.

(18) Najdi, R.; Proffitt, K.; Sprowl, S.; Kaur, S.; Yu, J.; Covey, T. M.; Virshup, D. M.; Waterman, M. L. A uniform human Wnt expression library reveals a shared secretory pathway and unique signaling activities. *Differentiation* **2012**, *84* (2), 203−213.

(19) Yap, M. C.; Kostiuk, M. A.; Martin, D. D.; Perinpanayagam, M. A.; Hak, P. G.; Siddam, A.; Majjigapu, J. R.; Rajaiah, G.; Keller, B. O.; Prescher, J. A.; Wu, P.; Bertozzi, C. R.; Falck, J. R.; Berthiaume, L. G. Rapid and selective detection of fatty acylated proteins using omega-alkynyl-fatty acids and click chemistry. *J. Lipid Res.* **2010**, *51* (6), 1566−1580.

(20) Balding, P. R.; Porro, C. S.; McLean, K. J.; Sutcliffe, M. J.; Marechal, J. D.; Munro, A. W.; de Visser, S. P. How do azoles inhibit cytochrome P450 enzymes? A density functional study. *J. Phys. Chem. A* **2008**, *112* (50), 12911−12918.

(21) Wassvik, C. M.; Holmen, A. G.; Bergstrom, C. A.; Zamora, I.; Artursson, P. Contribution of solid-state properties to the aqueous solubility of drugs. *Eur. J. Pharm. Sci.* **2006**, *29* (3−4), 294−305.

DOI: 10.1021/acs.jmedchem.5b00507
J. Med. Chem. XXXX, XXX, XXX−XXX